J Appl Electrochem (2010) 40:1605–1617
DOI 10.1007/s10800-010-0146-2

ORIGINAL PAPER

Adsorption and corrosion inhibition of amphiphilic compounds on steel pipeline grade API 5L X52 in sulphuric acid 1 M

Jonathán-Boanerge Pérez-Navarrete · C. O. Olivares-Xometl · N. V. Likhanova

Received: 12 May 2009 / Accepted: 25 April 2010 / Published online: 22 May 2010

Abstract The effect of seven amphiphilic compounds, on steel API 5L X52 corrosion in sulphuric acid 1 M solution was studied by potentiodynamic polarization curves, and electrochemical impedance spectroscopy (EIS). Potentiodynamic polarization curves indicated that these compounds acted mainly as cathodic type inhibitors. The EIS spectrums showed that the mechanism of corrosion inhibition is mainly a faradic process, the spectra were fitted with one electrical equivalent circuit (EEC) using a constant phase element (CPE). Double layer capacitance associated with CPE was also obtained. Langmuir, Temkin, and Henry adsorption isotherm described the experimental findings. This information suggested that organic molecules were adsorbed on active sites on metal surface avoiding contact of corrosive media with steel surface, having adsorbate molecules low molecular interaction between them even with the presence of more amphiphilic molecules on the steel surface as concentration got higher values.

J.-B. Pérez-Navarrete (✉)
División De Ciencias Básicas e Ingeniería, Universidad Autónoma Metropolitana, Unidad Azcapotzalco, Sn. Pablo No. 180, Sn. Pablo Xalpa, Azcapotzalco 02200, Mexico, DF, Mexico
e-mail: jbpn@xanum.uam.mx

C. O. Olivares-Xometl
Facultad de Ingeniería Química, Benemérita Universidad Autónoma de Puebla, Sur 104, Puebla 23354, Mexico, DF, Mexico

N. V. Likhanova
Programa de Ingeniería Molecular, Competencia de Química Aplicada, Instituto Mexicano del Petróleo, Eje Central Lázaro Cárdenas No. 152, San Bartolo Atepehuacan 07730, Mexico, DF, Mexico

Keywords Amphiphilic · Surfactant · Constant phase element · Steel pipeline grade API 5L X52 · Sulphuric acid · Corrosion inhibitor

Abbreviations

CI	Corrosion inhibitor(s)
MetTImBr	1-Methyl-3-tetradecylimidazolium bromide
MetHImBr	1-Methyl-3-hexadecylimidazolium bromide
TPyBr	N,N-Tetradecylpyridinium bromide
HPyBr	N,N-hexadecylpyridinium bromide
DMetEtBAmBr	N,N-Dimethyl-N-ethylbenzylammonium bromide
MetEtBAmLau	N,N-Dimethyl-N-ethylbenzylammonium laurite
DMetEtBAmAc	N,N-Dimethyl-N-ethylbenzylammonium acetate
Δ	Conventional Heating
MW	Microwaves
M.P.	Melting Point
Rp	Polarization resistance
MW	Microwave
η	Overpotential
j	Current density
j_a	Anodic current density
j_c	Cathodic current density
E_{corr}	Corrosion potential
j_{corr}	Corrosion current density
R	Constant of Gases
T	Absolute Temperature
b_c, b_a	Tafel Constants
C	Concentration
θ	Coverage degree

IE	Corrosion inhibition efficiency
rds	Rate-determining step
ΔG^0_{ads}	Adsorption free energy
K_{ads}	Equilibrium constant
f	Molecular interaction constant
ECC	Electrical equivalent circuit
CPE	Constant phase element
Rs	Solution resistance
Rct	Charge transfer resistance
C_{dl}	Capacitance of the double layer
ϕ	Phase angle
ϕ_{max}	Maximum value of phase angle in Bode Plot
ε_0	Vacuum permittivity
ε_r	Relative permittivity of dielectric
S	Surface of dielectric media
e	Thickness of dielectric media
C_{CPE}	Capacitance associated with the CPE

1 Introduction

Corrosion has a foremost economic impact. The replacement cost of damaged equipment is a significant capital expenditure. Unexpected outages decrease throughput, lowering earnings and profit [1]. The total cost of corrosion in every country in the world is estimated to be 2–5% GNP [2–4]. More essentially, corrosion is a main concern of the oil production due to the extremely dangerous nature of the fluids and gases, also extremes temperature and pressure encountered in deep gas wells. Temperatures near 230 °C have been present, and partial pressures of CO_2 and H_2S of the order of 20.7 and 48 MPa, respectively, have been encountered. The safety and well-being of plant equipment and employees are put at risk by corrosion. Catastrophic failures may perhaps result in severe damage to process units, neighbouring communities, and the surroundings. The methods of corrosion control commonly employed in petroleum production operations include: Proper selection of materials, protective coatings, cathodic protection systems, control of the environment, use of non-metallic materials and use of corrosion inhibitors (CI) [5, 6]. The role of inhibitors added in low concentrations to corrosive media, is to decrease or stop the reaction of the metal with the medium, inhibitors act by adsorption of ions or molecules onto the metal surface. They generally reduce the corrosion rate by blocking of the anodic and/or cathodic reaction. Several kinds of them had been used through the time [7–9]. Due to their characteristics, amphiphilic compounds have been used has CI [10–12], therefore in the present study, the efficiency of seven amphiphilic compounds for the inhibition of steel API 5L X52 corrosion in a 1 M H_2SO_4 solution was investigated. The amphiphilic compounds and their structures are shown in Table 1. Corrosion inhibition was investigated by means of potentiodynamic polarization curves and EIS.

2 Experimental details

The sample selected for the study was steel API 5L X52. The steel coupons used had the following composition (wt%): 0.08 C, 1.06 Mn, 0.26 Si, 0.019 P, 0.003 S, 0.0039 Al, 0.041 Nb, 0.018 Cs, 0.02 Cr, 0.019 Ni, 0.054 V, 0.003 Ti, 0.0002 Ca, 0.0003 B and the balance being Fe. The coupons were

Table 1 Chemical formulae of the investigated compounds

Name	Abbreviation	Cation	Anion	Molecular weight
1-Methyl-3-tetradecylimidazolium bromide	MetTImBr	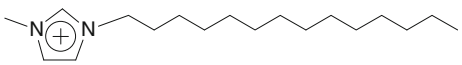	Br^-	$C_{18}H_{35}BrN_2$ 359.39
1-Methyl-3-hexadecylimidazolium bromide	MetHImBr	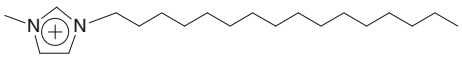	Br^-	$C_{20}H_{39}BrN_2$ 387.45
N,N-tetradecylpyridinium bromide	TPyBr	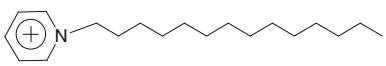	Br^-	$C_{19}H_{34}BrN$ 356.39
N,N-hexadecylpyridinium bromide	HPyBr	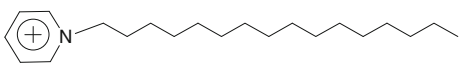	Br^-	$C_{21}H_{38}BrN$ 384.44
N,N-Dimethyl-N-ethylbenzylammonium bromide	DMetEtBAmBr	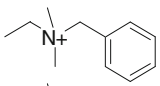	Br^-	$C_{11}H_{18}BrN$ 244.17
N,N-Dimethyl-N-ethylbenzylammonium laurite	DMetEtBAmLau	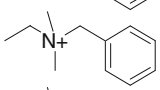	$CH_3(CH_2)_{10}COO^{\ominus}$	$C_{23}H_{41}NO_2$ 363.58
N,N-Dimethyl-N-ethylbenzylammonium acetate	DMetEtBAmAc	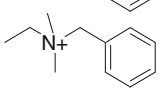	$CH_3COO^{\ominus}$	$C_{13}H_{21}NO_2$ 223.32

mechanically polished with different grades of emery paper, down to 1,200, degreased with acetone and dried. One Molar H_2SO_4 acid was used as the blank corrosion test solution. Commercial *N*-methylimidazol (99%, Aldrich), pyridine (99%, Aldrich), *N,N*-dimetiletilamine (99%, Aldrich), benzyl bromide (99%, Aldrich), 1-bromotetradecane (97%, Aldrich), 1-bromohexadecane (97%, Aldrich), lauric acid (98%, Aldrich), sodium ethoxide (21%, ethanol (Aldrich), acetonitrile, ethyl acetate and toluene were HPLS grade. Melting points were recorded on an Electrothermal-IA9000-Digital Melting Point Apparatus. IR spectra were recorded on a Nicolet FT-IR 5DX FT spectrometer. ^{1}H (300 MHz) and ^{13}C (75.4 MHz) NMR spectra were recorded on a Jeol Eclipse-300 NMR spectrometer (tetramethylsilane (TMS) as an internal standard). A microwave reactor, Discovery purchased from CEM Corporation, was used for synthesis of amphiphilic compounds. The microwave reactor was equipped with a magnetic stirrer and fitted with temperature and pressure probes. The concentration range of inhibitors was varied from 10 to 200 ppm. A three-electrode cell, employing a steel API 5L X52 electrode (sectional area 0.5 cm^2), graphite counter electrode, and Ag/AgCl reference electrode was used for measurements. Electrochemical measurements were performed using a potentiostat/galvanostat ZRA PC3 GAMRY, software packages CMS100 and CMS105 provided by GAMRY were used to obtain the polarization curves and electrochemical impedance spectra. The electrode was polarized from −250 to +250 mV versus E_{corr} at 0.125 mV s^{-1}. The cell was open to the laboratory air, and measurements were conducted at room temperature (295 ± 2 K). Also, the electrode was then polarized from −20 to +20 mV versus E_{corr} at 0.166 mV s^{-1} for polarization resistance measurements (Rp). Methods for synthesis of amphiphilic compounds were conventional heating (Δ) and microwave irradiation (MW; see Fig. 1).

2.1 Conventional

Synthesis of MetTImBr, N-methylimidazol (4.10 g, 50 mmol) and 1-bromidetetradecane (15.25 g, 55 mmol) were added to 50 mL of toluene. The preparation of the amphiphilic compounds via conventional heating method in refluxing solvents requires several hours. The mixture was stirred during 24 h. Upon completion of the reaction the lower phase was collected. This phase was washed twice with hexane. The crude product was recrystallized in ethyl acetate and the solvent was removed in vacuo. Synthesis of MetHImBr required addition of 1-bromidehexadecane (16.79 g, 55 mmol). However, for synthesis of TPyBr and HPyBr a mixture of pyridine (3.95 g, 50 mmol), toluene (50 mL) and 1-bromidetetradecane (15.25 g, 55 mmol) or 1-bromidehexadecane (16.79 g, 55 mmol) was required. The mixture was stirred during 30 h. Synthesis of DMetEtBAmBr was performed using a mixture of toluene (30 mL), *N,N*-dimetiletilamine (3.66 g, 50 mmol) and benzyl bromide (10.26 g, 60 mmol). The mixture was stirred during 5 h.

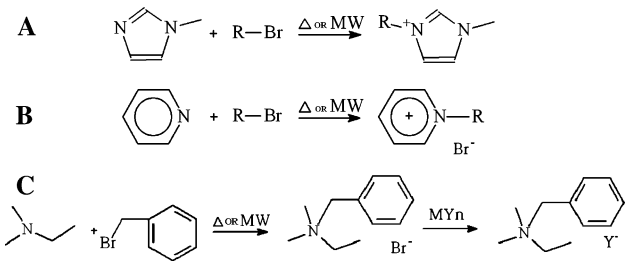

Fig. 1 **a** General reaction scheme for the synthesis of MetTImBr and MetHImBr. **b** General reaction scheme for the synthesis of TPyBr and HPyBr. **c** General reaction scheme for the synthesis of DMetEtBAmBr, DMetEtBAmLau and DMetEtBAmAc

2.2 MW synthesis

The mixture to produce MetTImBr and MetHImBr was irradiated at 25 W, programmed to ramp to 140 °C, and irradiation continued for 45 min. Synthesis of TPyBr and HPyBr was irradiated at 20 W, programmed to ramp to 110 °C, and irradiation continued for 1 h. Upon completion of the reaction same procedures was performed as described above. Synthesis of DMetEtBAmLau was performed with a mixture of DMetEtBAmBr and sodium laurite. The synthesis of sodium laurite requires neutralize a solution of ethanol (50 mL) and lauric acid (6.01 g, 30 mmol) with sodium ethoxide dissolved in ethanol (21%) at 77 °C. The solvent was removed in vacuo (105 °C). A mixture of DMetEtBAmBr (4.88 g, 20 mmol) and sodium laurite (4.45 g, 20 mmol) was placed in a reaction vessel equipped with a magnetic stirrer and fitted with temperature and pressure probes. The mixture was irradiated at 80 W, programmed to ramp to 100 °C, and irradiation continued for 1 h. The product was dissolved in dichloromethane and filtered. The synthesis of DMetEtBAmAc required a mixture of DMetEtBAmBr (4.88 g, 20 mmol) with ammonium acetate (1.54 g, 20 mmol).

2.2.1 MetTImBr

MetTImBr was obtained as a white solid. Conventional synthesis yield 92%; MW synthesis yield 91%. M.P.: 54–55 °C. IR (ATR, cm^{-1}) 3485, 3058, 2910, 2842, 1630, 1575, 1472, 1180. ^{1}H NMR (300 MHz, $CDCl_3$) δ (ppm): 10.08–10.23 (s, $J = 14$ Hz), 7.41–7.68 (d, $J = 8.4$ Hz, 2H), 4.30–4.35 (t, $J = 6.4$ Hz, 3H), 1.86–1.95 (m, 5H), 1.25–1.33 (m, 13H). 0.85–0.90 (t, $J = 6.4$ Hz, 3H), 4.13 (s, $J = 14$ Hz). ^{13}C NMR (75.4 MHz, $CDCl_3$) δ (ppm): 122.0–123.8, 137.0, 50.1, 22.6–36.8 (5C), 14.0.

2.2.2 MetHImBr

MetHImBr was obtained as a white solid. Conventional synthesis yield 93%; MW synthesis yield 92%. M.P.: 61–62 °C. IR (ATR, cm^{-1}) 3486, 3058, 2910, 2844, 1630, 1575, 1474, 1182. ^{1}H NMR (300 MHz, $CDCl_3$) δ (ppm): 10.08–10.23 (s, $J = 14$ Hz), 7.41–7.68 (d, $J = 8.4$ Hz, 2H), 4.30–4.35 (t, $J = 6.4$ Hz, 3H), 1.86–1.95 (m, 5H), 1.25–1.33 (m, 13H). 0.85–0.90 (t, $J = 6.4$ Hz, 3H), 4.13 (s, $J = 14$ Hz). ^{13}C NMR (75.4 MHz, $CDCl_3$) δ (ppm): 122.0–123.8, 137.0, 50.1, 22.6–36.8 (5C), 14.0.

2.2.3 TPyBr

TPyBr was obtained as a yellow solid. Conventional synthesis yield 89%; MW synthesis yield 87%. M.P.: 50–52 °C. IR (ATR, cm^{-1}) 3408, 2910, 2848, 1645, 1474, 1171, 781, 684. ^{1}H NMR (300 MHz, $CDCl_3$) δ (ppm): 8.54–8.56 (m, 6H), 8.21–8.16 (m, 6H), 9.45–9.48 (dd, $J1 = 9.0$ Hz, $J2 = 4.8$ Hz, 2H), 4.95–5.00 (t, $J = 6.2$ Hz, 3H) 2.02–2.07 (m, 5H), 1.23–1.33 (m, 3H), 0.85–0.9 (t, $J = 7.2$ Hz, 3H). ^{13}C NMR (75.4 MHz, $CDCl_3$) δ (ppm): 145.3–145.5, 145.1, 128.6, 61.2–62.2, 22.7–32.0 (5C), 14.1.

2.2.4 HPyBr

HPyBr was obtained as a white waxy solid. Conventional synthesis yield 90%; MW synthesis yield 89%. M.P.: 58–60 °C. IR (ATR, cm^{-1}) 3405, 2922, 2848, 2112, 1638, 1478, 1178, 781. ^{1}H NMR (300 MHz, $CDCl_3$) δ (ppm): 8.54–8.56 (m, 6H), 8.21–8.16 (m, 6H), 9.45–9.48 (dd, $J1 = 9.0$ Hz, $J2 = 4.8$ Hz, 2H), 4.95–5.00 (t, $J = 6.2$ Hz, 3H) 2.02–2.07 (m, 5H), 1.23–1.33 (m, 3H), 0.85–0.9 (t, $J = 7.2$ Hz, 3H). ^{13}C NMR (75.4 MHz, $CDCl_3$) δ (ppm): 145.3–145.5, 145.1, 128.6, 61.2–62.2, 22.7–32.0 (5C), 14.1.

2.2.5 DMetEtBAmBr

DMetEtBAmBr was obtained as a white solid. Conventional synthesis yield 95%; M.P.: 155–157 °C. IR (ATR, cm^{-1}) 3428, 3015,297.3, 1478, 1431, 1213, 1027, 819, 781, 723. ^{1}H NMR (300 MHz, D_2O) δ (ppm): 7.51 (m, 2H), 4.41 (s, $J = 12$ Hz), 3.31–3.38 (m, 3H), 2.94 (s, $J = 12$ Hz), 1.37–1.42 (m, 3H). ^{13}C NMR (75.4 MHz, D_2O) δ (ppm): 133.2–127.5, 67.5, 60.1, 49.2, 7.9.

2.2.6 DMetEtBAmLau

DMetEtBAmLau was obtained as a white dense liquid. MW synthesis yield 85%. IR (ATR, cm^{-1}) 3455, 2922, 2840, 1719, 1470, 1221, 875, 723. ^{1}H NMR (300 MHz, $CDCl_3$) δ (ppm): 7.51 (m, 2H), 4.41 (s, $J = 12$ Hz), 3.31–3.38 (m, 3H), 2.94 (s, $J = 12$ Hz), 1.37–1.42 (m, 3H), 2.2 (t, $J = 6.$ 2 Hz, 3H), 1.54 (qi, $J = 7.2$ Hz, 1H), 1.24 (m, 5H), 0.88 (t, $J = 6.2$ 3H). ^{13}C NMR (75.4 MHz, $CDCl_3$) δ (ppm):178.9, 133.2–127.5, 67.5, 60.1, 49.2, 31.9, 22.7, 26.1–29.7, 14.1, 7.9.

2.2.7 DMetEtBAmAc

DMetEtBAmAc was obtained as a yellow solid. MW synthesis yield 89%. M.P.:149–151 °C. IR (ATR, cm^{-1}) 3428, 2980, 2077, 1630, 1486, 1412, 1217, 1019, 859, 723. ^{1}H NMR (300 MHz, $CDCl_3$) δ (ppm): 7.51 (m, 2H), 4.41 (s, $J =$ 12 Hz), 3.31–3.38 (m, 3H), 2.94 (s, $J = 12$ Hz), 1.37–1.42 (m, 3H), 1.98 (s, $J = 12$ Hz). ^{13}C NMR (75.4 MHz, $CDCl_3$) δ (ppm): 175.1, 133.2–127.5, 67.5, 60.1, 49.2, 23.3, 7.9.

3 Results and discussion

3.1 Synthesis

The synthesis of amphiphilic compounds was performed in two steps: formation of the desired cation and anion exchange to obtain the desired product. The first step involves an alkylated halide precursor of the amphiphilic compound, and sometimes a second step: metathesis, to obtain desired anion. Using conventional heating methods is time-consuming (2–48 h), besides usually requires a large molar excess of haloalkane to achieve good yields [13, 14]. Microwave-assisted synthesis of amphiphilic compounds was performed in <2 min and yields were found over 85%. This is in agreement with the experimental results [15–21].

3.2 Polarization curves

Steel API 5L X52 samples were immersed at 298 K in 1 M H_2SO_4 solution at various contents of amphiphilic compounds. The cathodic and anodic polarization curves with concentration of MetTImBr and TPyBr are shown in Fig. 2a and b (polarization curves without and in the presence of different concentrations of tested CI, were similar in shape). In the presence of CI, the cathodic and anodic curves were shifted and the shift was dependent on CI concentration, possibly due to spatial reorientation during adsorption onto steel surface of more available molecules of CI. The addition of CI leads to a decrease in the current densities. Inhibition of corrosion and the reduction in current density observed was due to the inhibitor performance, Lorenz, and Mansfeld have pointed out that corrosion inhibition is linked with [22]: (1) geometric blocking of the species adsorbed in active sites on metal surface, (2) blocking the active sites for the species adsorbed on them, or (3) electrocatalytic effect of the inhibitor or its products, however, the latter seems unlikely,

the addition of CI to the corrosive solution did not modify the cathodic Tafel slope or the anodic Tafel slope (b_c and b_a), thus the mechanism of the processes was not affected. The decrease in current density with the inhibitor concentration is associated with a shift of corrosion potential E_{corr} to more negative values, indicating that amphiphilic compounds act as cathodic type inhibitors [22–31]. The approximately constant values of the Tafel slopes suggest that the inhibition mechanism for amphiphilic compounds involves a single reaction site blocking. The mechanism of adsorption of inhibitor molecules on the surface often involves the movement of water molecules absorbed, which are replaced by the inhibitor molecules and in contact with the metal surface are adsorbed as is shown in Eq. 1 [22, 23]:

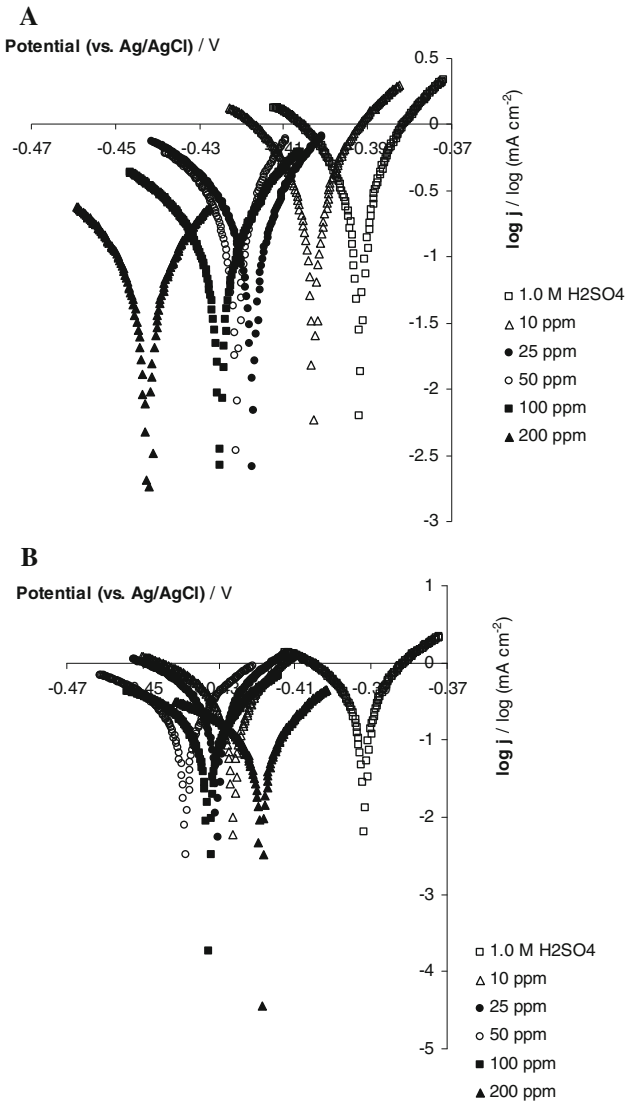

Fig. 2 **a** Tafel curves at different concentrations of MetTImBr (log j vs. V (Ag/AgCl)/V) for steel API 5L X52 in H_2SO_4 1 M. **b** Tafel curves at different concentrations of TPyBr (log j vs. V (Ag/AgCl)/V) for steel API 5L X52 in H_2SO_4 1 M

$$\mathrm{Fe} + \mathrm{Inh} \leftrightarrow \mathrm{Fe(Inh)}_{ads} \leftrightarrow \mathrm{Fe}^{n+} + ne^- + \mathrm{Inh}. \quad (1)$$

The main mechanism of action for a cathodic inhibitor is reduction of cation in solution forming an insulating layer which deposits on the cathodic part of the corroding surface (Fig. 3). The corrosion potential becomes more cathodic because reduces the anodic dissolution [32, 33]. According to Bockris and others, the dissolution mechanism to explain dissolution of iron (BDD mechanism) [34] using an intermediate that plays a key role because involves only one single electron transfer and using the stoichiometric number of unity for the rate-determining step (rds); according to this, Fig. 4 shows the corroding steel surface reactions in the presence of amphiphilic compounds [35]; for instance, TPyBr. The overall reaction mechanism proceeds in four stages. In stage I: corroding steel continues providing ions Fe^{+2} to solution; during stage II: $(OH)^-$ combines with corroding Fe and TPyBr to form two intermediates this reduction of cation of amphiphilic compound causes shifting of E_{corr} to cathodic values; during stage III: intermediates formed in stage II are adsorbed on metal surface avoiding in this manner corrosion $(TPy(OH))_{ads}$, but the presence of $(Fe(OH))_{ads}$ continues with corrosion process; during stage IV: take place desorption of intermediates and the process may starts again with stage I.

Resistance to polarization (Rp) values were obtained from the Tafel curves [36]. Values of associated electrochemical parameters and corrosion inhibition efficiency (IE), corrosion current density (j_{corr}) and surface coverage degree (θ) are given in Table 2. IE, j_{corr} and θ were obtained from the Eqs. 2–4 [35–38]:

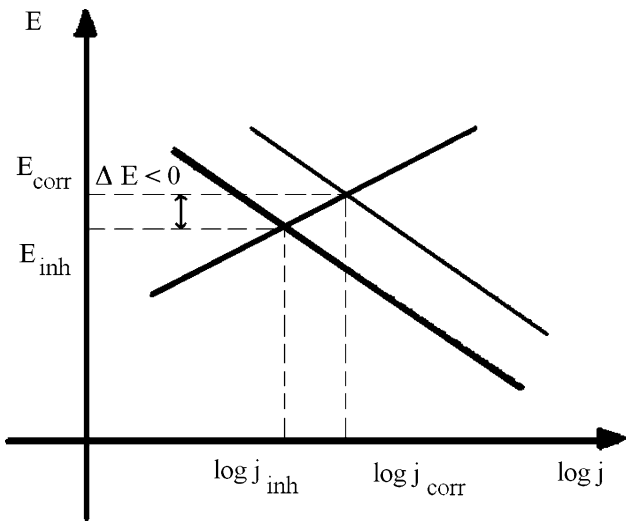

Fig. 3 Potential shifting caused by cathodic inhibitor presence in corrosive media

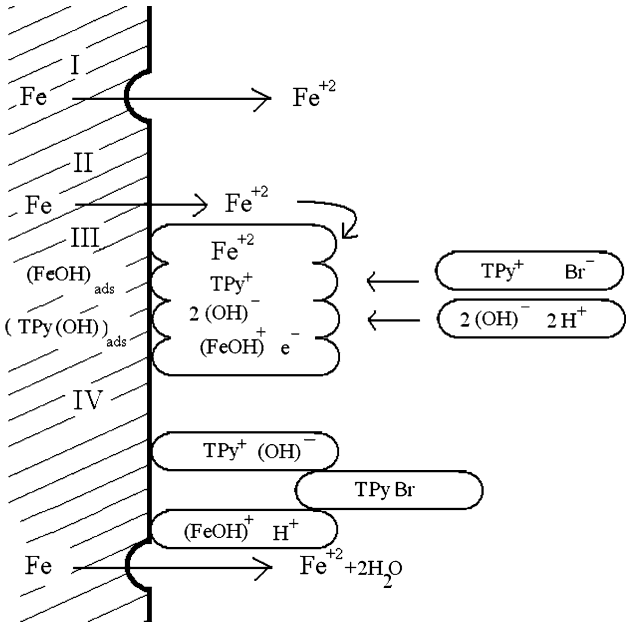

Fig. 4 Schematic representation of reactions in the inhibition of corrosion by TPyBr for steel API 5L X52 in H_2SO_4 1 M

$$\mathrm{IE} = \left(1 - \frac{(\mathrm{R_p})_t}{(\mathrm{R_p})_{inh}}\right) \times 100 \tag{2}$$

$$j_{corr} = \frac{b_a b_c}{2.3Rp(b_a + b_c)} \tag{3}$$

$$\theta = 1 - \frac{(R_p)_t}{(R_p)_{inh}}. \tag{4}$$

The subscript t means absence of inhibitor, inh indicates the presence of inhibitor. Figure 5 shows the plot of the IE against the concentration of amphiphilic compounds. Inspection of these data reveals that the presence of shortest alkyl chain for compounds with cation structure of methyl-alkyl-imidazolium: over 50 ppm increased dramatically the IE (78.4%). The adsorption could be via the nitrogen atoms of the heterocyclic five-membered ring molecule of MetTImBr and MetHImBr, these CI are cationic to some extent; i.e., they carry a positive electrical charge in the heterocyclic five-membered ring. Also shall be noted that at 25 ppm MetTImBr and MetHImBr compounds reached a maximum, produced by steric hindrance of alkyl chain which created a spatial rearrangement of molecules to minimize energy [39], which allowed more arriving molecules to be adsorbed onto metallic surface. The compounds TPyBr and HPyBr have one nitrogen atom, therefore adsorption was linked to interaction of π-bonds and vacant d orbitals of superficial iron atoms [40], and thus steric hindrance of alkyl chain was less important for TPyBr and HPyBr. Therefore, the longer alkyl chain at concentrations below 50 ppm increased IE in HPyBr. At all concentration, tested molecules with pyridium ring had higher IE than those with the imidazolium ring. However, compounds DMetEtBAmBr, DMetEtBAmLau and DMetEtBAmAc showed superior IE, this is probably due to the influence of the aromatic ring in their structure. Differences in IE of the last three CI were related to the presence of the same cation but different anion (Table 1). Although the anions of DMetEtBAmLau and DMetEtBAmAc could protonate [41], and IE was grater for DMetEtBAmAc, possibly protonation was faster in solution for DMetEtBAmAc and produced higher IE, because DMetEtBAmAc had a lower hydrophobic character than DMetEtBAmLau. The corrosion inhibition study indicated that DMetEtBAmBr had the highest IE compared to other amphiphilic compounds. The reason of the value 76.7% of IE with a deviation of 3.5% for DMetEtBAmLau was linked with hydrophobic character of anion that in solution avoided charge transport. Anion protonation could also explain the similar values of E_{corr} for DMetEtBAmAc (Table 2) which produced similar availability of protons for interfacial reactions. The corrosion inhibition property of the amphiphilic compounds can be attributed to the presence of heteroatoms, such as N and of π-electrons on aromatic nuclei, even though these factors play the vital role in the adsorption of the CI on the metal surface performance of compounds showed that higher IE is enhanced by π-bonds rather than the presence of N, and protonation of anion coupled to cation in the inhibitor molecule. The presence of longer or shorter alkyl chain may increase o diminish IE, but depends strongly in the concentration of CI and also in the heteroatoms and π-electrons in the chemical structure of molecule.

3.3 Adsorption isotherm

The adsorption process involves the displacement of water molecules from the metal surface. Ten adsorption isotherms (Langmuir, Temkin, Freundlich, Frumkin, Modified Langmuir, Henry, Viral, Damaskin, Volmer and Flory–Huggins) [42, 43] were tested for their fit to the experimental data. The best approach for MetTImBr, MetHImBr, TPyBr and HPyBr (Fig. 6) was obtained with the Langmuir adsorption isotherm. On the other hand, the Temkin adsorption isotherm (Fig. 7) was the best for DMetEtBAmBr and Henry adsorption isotherm fitted closely experimental data for DMetEtBAmAc (Fig. 8). These isotherms are represented by Eqs. 5–7:

Langmuir

$$K_{ads}C = \frac{\theta}{1-\theta} \tag{5}$$

Temkin

Table 2 Electrochemical parameters of the corrosion data of steel API 5L X52 in 1 M H_2SO_4 in the presence of MetTImBr, MetHImBr, TPyBr, HPyBr, DMetEtBAmBr, DMetEtBAmLau and DMetEtBAmAc

	Inhibitor concentration/C (ppm)	E_{corr} (mV)	j_{corr} (μA cm^{-2})	b_c (mV decade^{-1})	b_a (mV decade^{-1})	Rp (Ω cm^2)	θ (/)	IE (%)
	0	−391.9	473.1	36.6	24.4	13.4	–	–
MetTImBr	10	−402.9	267.2	36.5	24.4	23.8	0.435	43.5
	25	−417.3	224.8	36.7	24.5	28.4	0.527	52.7
	50	−421.1	276.5	36.9	24.3	23.0	0.416	41.6
	100	−425.1	141.1	36.7	24.7	45.4	0.704	70.4
	200	−442.2	101.8	36.4	24.4	62.3	0.784	78.4
MetHImBr	10	−412.1	281.0	36.8	24.3	22.6	0.406	40.6
	25	−419.4	210.6	36.7	24.0	29.9	0.551	55.1
	50	−416.7	270.9	36.5	24.4	23.4	0.427	42.7
	100	−409.5	221.4	36.3	24.4	28.6	0.530	53.0
	200	−420.0	167.4	36.5	24.1	37.7	0.643	64.3
TPyBr	10	−426.4	312.7	36.7	24.2	20.3	0.36	33.6
	25	−430.3	288.9	36.6	24.3	22.0	0.388	38.8
	50	−438.8	285.4	36.1	24.4	22.1	0.393	39.3
	100	−432.7	175.7	36.5	24.8	36.5	0.632	63.2
	200	−420.0	99.1	36.7	24.8	64.9	0.793	79.3
HPyBr	10	−438.8	139.3	36.4	24.5	45.7	0.706	70.6
	25	−434.6	175.1	36.6	24.5	36.4	0.631	63.1
	50	−428.5	158.7	36.4	24.8	40.4	0.667	66.7
	100	−432.1	141.3	36.2	24.8	45.2	0.703	70.3
	200	−419.6	88.5	36.9	25.0	73.1	0.816	81.6
DMetEtBAmBr	10	−430.0	155.0	36.5	24.2	40.8	0.670	67.0
	25	−434.4	124.6	36.7	24.2	50.8	0.736	73.6
	50	−431.1	113.6	36.7	24.2	55.7	0.759	75.9
	100	−440.2	93.5	36.2	24.4	67.7	0.802	80.2
	200	−437.4	70.3	36.2	24.5	90.3	0.851	85.1
DMetEtBAmLau	10	−427.7	128.0	36.4	24.4	49.6	0.729	72.9
	25	−426.1	113.5	36.2	24.2	55.5	0.758	75.8
	50	−430.2	100.1	36.8	24.5	63.8	0.789	78.9
	100	−439.9	111.7	36.2	24.5	56.8	0.763	76.3
	200	−440.7	96.6	36.4	24.4	65.6	0.795	79.5
DMetEtBAmAc	10	−441.2	110.7	34.3	24.5	56.1	0.760	76.0
	25	−441.2	108.1	34.4	24.4	57.3	0.766	76.6
	50	−439.5	96.3	35.4	23.1	63.1	0.787	78.7
	100	−440.7	89.8	34.6	20.7	62.5	0.785	78.5
	200	−439.5	62.2	35.8	18.6	85.4	0.843	84.3

$$K_{ads}C = e^{f\theta} \quad (6)$$

Henry

$$K_{ads}C = \theta \quad (7)$$

Molecules of MetTImBr, MetHImBr, TPyBr and HPyBr for steel API 5L X52 occupied an active site, interactions between the inhibitor molecules were negligible and once molecules were adsorbed, molecules formed a monolayer [44–51] onto steel surface. The presence of Br^- ions in aqueous solution could have a synergistic effect of the adsorption process, creating an excess negative charge towards the solution that enhanced the adsorption of cations on surface [52]. Adsorption free energy (ΔG^0_{ads}) is given by Eq. 8 [11]:

$$\Delta G^0_{ads} = -RT\ln(K_{ads}). \quad (8)$$

The value of Free energy of adsorption for MetTImBr, MetHImBr, TPyBr and HPyBr compounds was about −20.7 kJ mol^{-1} (Table 3), therefore adsorption of these

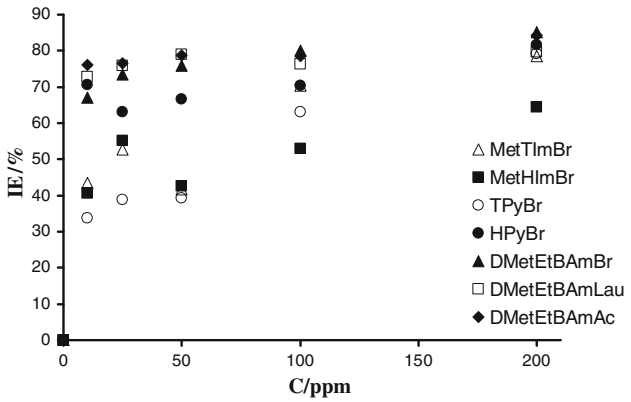

Fig. 5 Variation of corrosion inhibition efficiency (IE/%) with concentration (C/ppm) of amphiphilic compounds for the steel API 5L X52 in 1 M H_2SO_4

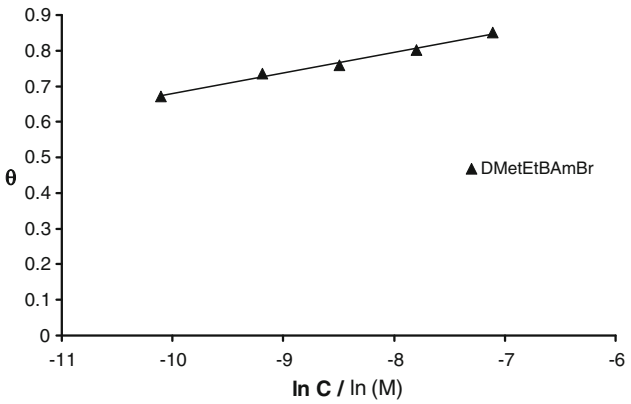

Fig. 7 Curve fitting of the corrosion data of steel API 5L X52 in 1 M H_2SO_4 in the presence of DMetEtBAmBr to Temkin isotherm

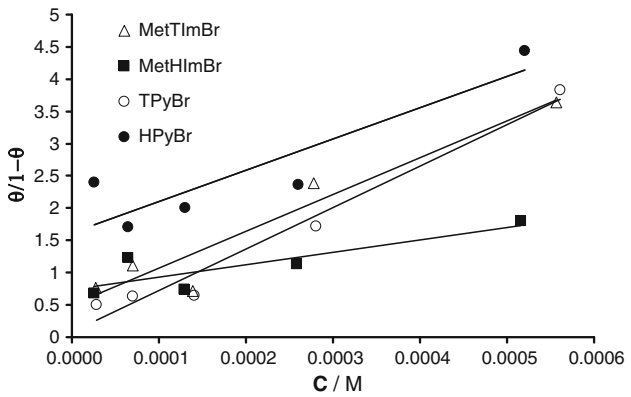

Fig. 6 Curve fitting of the corrosion data of steel API 5L X52 in 1 M H_2SO_4 in presence of MetTImBr, MetHImBr, TPyBr and HPyBr to Langmuir isotherm

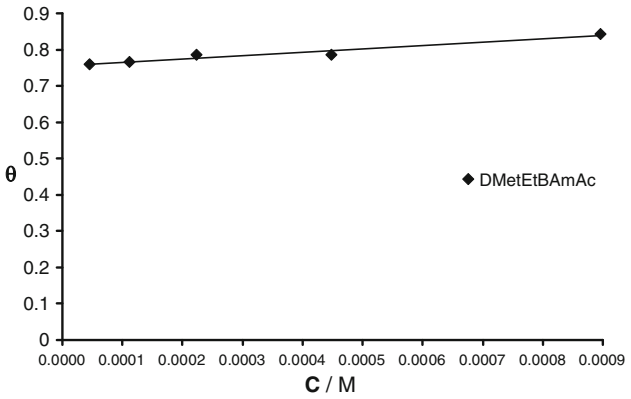

Fig. 8 Curve fitting of the corrosion data of steel API 5L X52 in 1 M H_2SO_4 in presence of DMetEtBAmAc to Henry isotherm

compounds was physisorption [46]. Greater values of ΔG^0_{ads} and K_{ads} says little about film stability of inhibiting layer, since ΔG^0_{ads} or K_{ads} do not contain information about kinetic of process during corrosion inhibition.

Thus, Temkin adsorption isotherm (DMetEtBAmBr) suggests that the adsorption process was governed by the heterogeneity of the surface. ΔG^0_{ads} had a value of -53.8 kJ mol^{-1} (Table 3), therefore adsorption process was chemisorption [53], the elevated value of parameter *f* relates the variation of energy over different zones (patches) of a heterogeneous surface showed that there were great differences in bonding of adsorbed molecules onto steel (Fig. 7).

Henry adsorption isotherm [54] is shown in Fig. 8. For this isotherm, there was a constant ratio between concentration and coverage (Fig. 8). The behaviour of DMetEtBAmAc could be explained by great affinity between adsorbate and adsorbent molecules, particularly in

Table 3 Adsorption isotherm, equilibrium constant, interaction constant and free energy of adsorption for steel API 5L X52 determined in a 1 M H_2SO_4 aqueous solution

Corrosion inhibitor	Adsorption isotherm	Equilibrium constant (K_{ads})	Interaction constant (*f*)	ΔG^0_{ads} (KJ mol^{-1})
MetTImBr	Langmuir	5697.4	*	−21.4
MetHImBr	Langmuir	1938.9	*	−18.8
TPyBr	Langmuir	6433	*	−21.7
HPyBr	Langmuir	4848.3	*	−21.0
DMetEtBAmBr	Temkin	2.67×10^9	17.2	−53.8
DMetEtBAmAc	Henry	91.4	*	−11.2

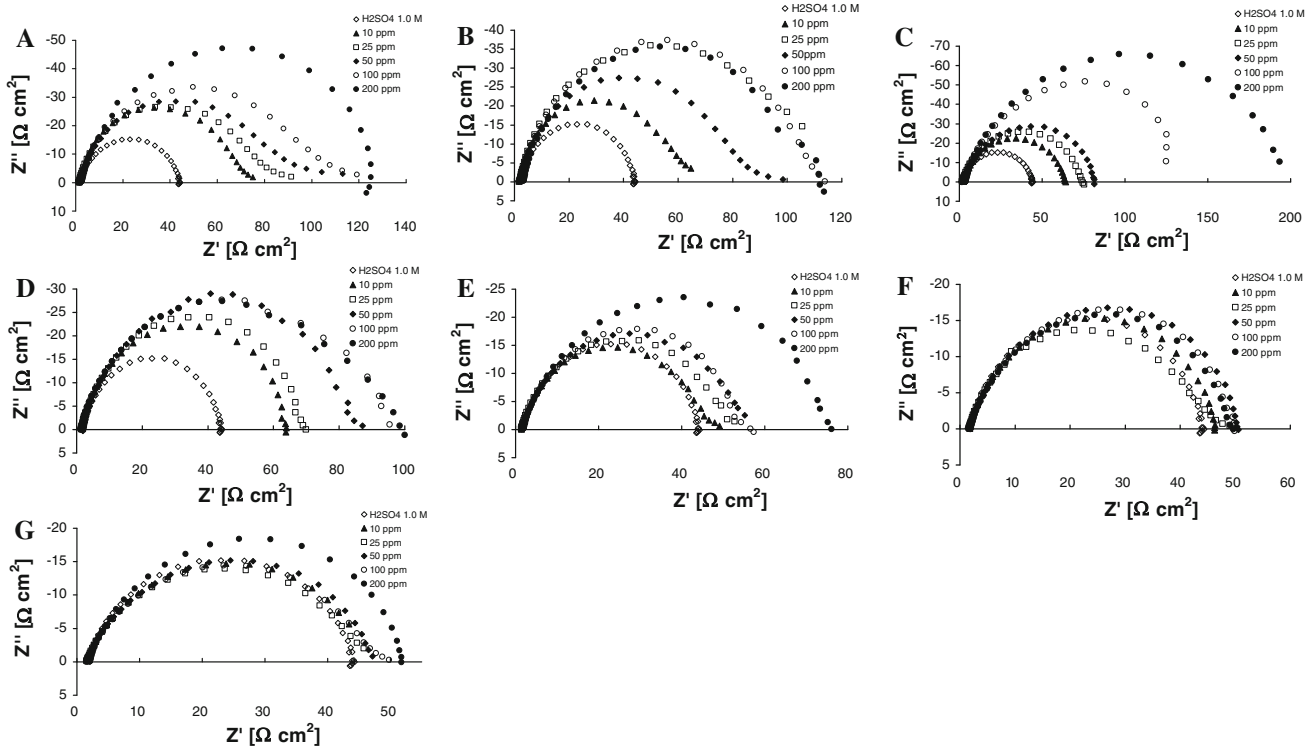

Fig. 9 Nyquist diagrams of steel API 5L X52 at different concentrations of inhibitor **a** MetTImBr in 1 M H_2SO_4, **b** MetHImBr in 1 M H_2SO_4, **c** TPyBr in 1 M H_2SO_4, **d** HPyBr in 1 M H_2SO_4, **e** DMetEtBAmBr in 1 M H_2SO_4, **f** DMetEtBAmLau in 1 M H_2SO_4 and **f** DMetEtBAmAc in 1 M H_2SO_4

some special zones in the adsorbent surface known as Henry's Zones [55]. This process can consist of three stages [56]: (1) a kinetic process ($0 \leq \theta \leq 0.5$) in the Henry's Zones, (2) a kinetic–diffusive process and (3) a diffusive process at the same time as concentration of CI was higher.

3.4 Electrochemical impedance spectroscopy (EIS)

Nyquist plots of steel in 1 M H_2SO_4 inhibited and uninhibited solutions containing various concentrations of amphiphilic compounds are shown in Fig. 9a–g.

The locus of Nyquist plots looks like one part of a semicircle. The results can be interpreted in terms of the EEC (Fig. 10), even if inductive loop was shown in a few spectra it was very small and EEC fitted well experimental data. The inductive loop is characteristic of corrosion in sulphuric acid [57–65], and is related to the pseudocapacitance of corrosion products adsorbed on corroded surface, the pseudocapacitance of corrosion products adsorbed on corroded surface, electrical elements of the circuit during the EIS test: as the counter electrode, the working electrode, the Luggin capillarity, the reference electrode, the electrolyte resistance and even the distance between reference electrode and the specimen, nonlinearity of the system at low frequency [61] and relaxation in dielectric media at low frequencies [63] (Fig. 10).

The impedance diagrams obtained were not perfect semicircles, therefore EEC used a CPE. The CPE impedance (Z_{CPE}, Eq. 8) is almost always used in an ad hoc manner to cause an EEC to fit the experimental data. For example, CPE's are often invoked to account for "depressed semicircles" (impedance loci in which the centre of the semicircle in the Nyquist plane is located below the real axis), following similar applications in dielectric relaxation studies. For CPE, Y_0 is a proportional factor; n has the meaning of a phase shift. In the CPE, the values of n can be: 1, 0.5, 0 and −1, therefore the CPE corresponds to different electrical elements: a capacitor, infinite Warburg impedance, resistor, and inductor, respectively.

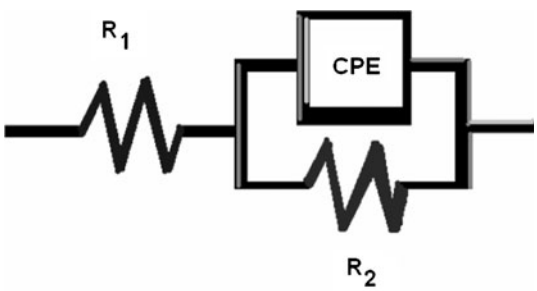

Fig. 10 Electrical equivalent circuit used to fit experimental data

$$Z_{\mathrm{CPE}} = \frac{Y_0^{-1}}{(j\omega)^n}. \quad (8)$$

The CPE is associated with the use of a solid electrode, in which the flattening is caused by a dispersion of frequency, this behaviour is typical of solid electrodes and is usually attributed to roughness and inhomogeneities of the electrode surface, resulting in a roughness of the coupling strength of solution and the surface capacitance and the capacitive surface scattering caused by the slow adsorption of ions. Rs, Solution Resistance (R_1). Rct, Charge Transfer Resistance (R_2). C_{dl}, Capacitance associated with the CPE (C_{CPE}) values are given in Table 4. The Rct and Rp values determined using the polarization curves were different than those determined by EIS experiments. This difference is probably due to the shorter immersion time in the case of the polarization measurements. Using the total impedance of the EEC, the C_{CPE} was derived according to next equations:

$$Z = R_1 + \frac{R_2}{1 + R_2 Y_0 (j\omega)^n} \quad (9)$$

Table 4 Parameters of the ECC of steel API 5L X52 at different concentrations of inhibitor in 1 M H_2SO_4

	Inhibitor concentration/C (ppm)	R_1 (Ω cm^2)	Y_o (S-s^n)	n	R_2 (Ω cm^2)	C_{CPE} (μF)
	0	1.658	1.486×10^{-4}	0.7965	42.7	40.8
MetTImBr	10	1.524	6.780×10^{-5}	0.8654	69.6	29.5
	25	1.287	8.095×10^{-5}	0.8378	79.1	30.4
	50	1.967	1.059×10^{-4}	0.7953	92.6	32.2
	100	1.778	1.060×10^{-4}	0.8056	103.3	35.7
	200	2.483	1.014×10^{-4}	0.8100	127.5	36.6
MetHImBr	10	1.663	9.338×10^{-5}	0.8380	59.5	34.2
	25	1.891	9.001×10^{-5}	0.8300	101.5	34.4
	50	1.640	1.133×10^{-4}	0.8008	84.4	35.6
	100	1.950	1.109×10^{-4}	0.8086	106.9	38.8
	200	3.178	1.293×10^{-4}	0.7962	105.4	43.1
TPyBr	10	2.447	1.162×10^{-4}	0.8090	61.7	36.2
	25	1.834	1.254×10^{-4}	0.7929	73.6	36.9
	50	2.828	1.175×10^{-4}	0.8036	79.8	37.5
	100	2.737	1.072×0^{-4}	0.7950	136.2	36.0
	200	3.571	1.141×10^{-4}	0.7982	189.2	43.3
HPyBr	10	1.455	1.334×10^{-4}	0.7995	63.3	40.3
	25	1.828	1.140×10^{-4}	0.8080	67.3	35.8
	50	1.839	1.267×10^{-4}	0.7955	81.9	39.1
	100	1.225	1.564×10^{-4}	0.7787	89.4	46.5
	200	1.222	1.597×10^{-4}	0.7763	90.3	47.1
DMetEtBAmBr	10	1.390	1.901×10^{-4}	0.7804	44.8	49.7
	25	1.300	1.853×10^{-4}	0.7767	49.2	48.0
	50	1.804	1.734×10^{-4}	0.7787	52.0	45.5
	100	1.793	1.594×10^{-4}	0.7765	53.1	40.4
	200	1.628	2.222×10^{-4}	0.7383	74.7	52.0
DMetEtBAmLau	10	1.695	1.698×10^{-4}	0.7801	44.9	42.9
	25	1.599	2.139×10^{-4}	0.7684	43.8	52.4
	50	1.759	1.791×10^{-4}	0.7729	49.2	44.6
	100	1.857	2.050×10^{-4}	0.7668	48.5	50.4
	200	1.640	2.504×10^{-4}	0.7408	48.6	53.6
DMetEtBAmAc	10	1.620	2.110×10^{-4}	0.7663	44.0	50.6
	25	1.476	2.414×10^{-4}	0.7470	43.8	51.7
	50	1.568	2.194×10^{-4}	0.7551	45.9	49.4
	100	1.675	2.525×10^{-4}	0.7461	45.9	55.4
	200	2.042	2.582×10^{-4}	0.8050	50.6	90.3

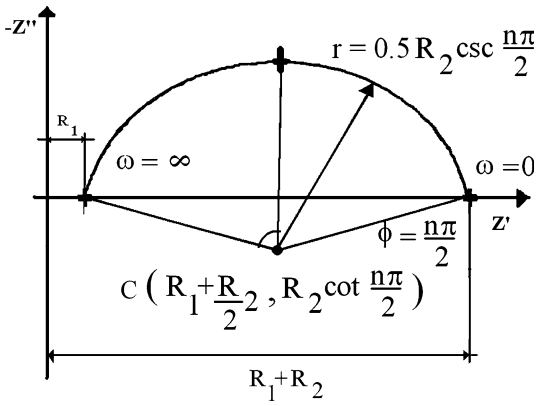

Fig. 11 Nyquist plot showing characteristic depressed semi-circle of CPE

$$(j\omega)^n = \omega^n e^{j\frac{n\pi}{2}} = \omega^n\left(\cos\frac{n\pi}{2} + j\,\mathrm{sen}\frac{n\pi}{2}\right). \tag{10}$$

Inserting Eq. 9 into Eq. 10, we obtain:

$$Z = R_1 + \frac{R_2}{1 + R_2 Y_0 \omega^n\left(\cos\frac{n\pi}{2} + j\,\mathrm{sen}\frac{n\pi}{2}\right)}$$
$$= R_1 + \frac{R_2 + R_2^2 Y_0 \omega^n \cos\frac{n\pi}{2} - jR_2^2 Y_0 \omega^n\,\mathrm{sen}\frac{n\pi}{2}}{1 + 2R_2 Y_0 \omega^n \cos\frac{n\pi}{2} + (R_2 Y_0 \omega^n)^2}. \tag{11}$$

And, separating the real and imaginary parts, if $Z = Z' + jZ''$, we can get the following relations:

$$-Z'' - \frac{R_2}{2}\tan\frac{n\pi}{2} = \left(\frac{R_2}{2}\right)\frac{-\left(1 + R_2^2(Y_0\omega^n)^2\right)\tan\frac{n\pi}{2}}{1 + 2R_2 Y_0 \omega^n \cos\frac{n\pi}{2} + (R_2 Y_0 \omega^n)^2} \tag{12}$$

$$Z' - R_1 - \frac{R_2}{2} = \left(\frac{R_2}{2}\right)\frac{\left(1 - R_2^2(Y_0\omega^n)^2\right)}{1 + 2R_2 Y_0 \omega^n \cos\frac{n\pi}{2} + (R_2 Y_0 \omega^n)^2}. \tag{13}$$

Taking the square of Eq. 13 and inserting Eq. 12 and using value of Z'' (of Eq. 11), after simplifications:

$$\left(Z' - R_1 - \frac{R_2}{2}\right)^2 + \left(-Z'' + R_2\cot\frac{n\pi}{2}\right)^2 = \left(\frac{R_2}{2}\csc\frac{n\pi}{2}\right)^2. \tag{14}$$

This is the equation of the depressed semicircle (Fig. 11). C_{dl} can be obtained at center C $\left(R_1 + \frac{R_2}{2}, R_2\cot\frac{n\pi}{2}\right)$, the maximum in the Nyquist plot when $Z' = R_1 + \frac{R_2}{2}$, Equation 15 reveals that it happens if $1 - R_2^2\left(Y_0\omega_{\max}^n\right)^2 = 0$, the unique solution in agreement with such condition implies that $R_2 Y_0 \omega^n = 1$, thus:

$$\omega^n = \frac{1}{R_2 Y_0} \tag{15}$$

The capacitance associated with the CPE (C_{CPE}) can be written using Eq. 15 as:

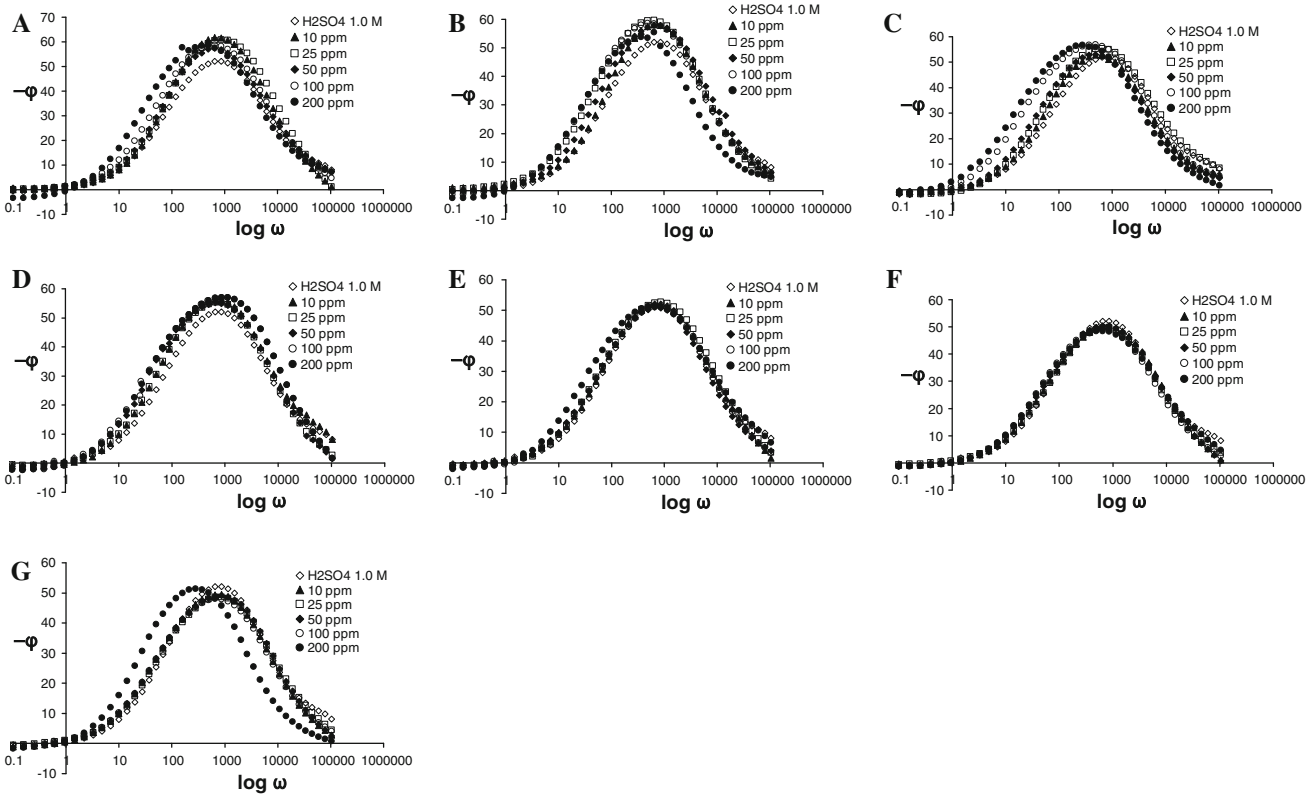

Fig. 12 Bode plot, phase angle versus frequency for steel API 5L X52 in 1 M H_2SO_4 at different concentration of inhibitor **a** MetTImBr, **b** MetHImBr, **c** TPyBr, **d** HPyBr, **e** DMetEtBAmBr, **f** DMetEtBAmLau and **g** DMetEtBAmAc

$$C_{CPE} = \frac{\tau}{R_2} = \frac{1}{\omega_{\max} R_2} = \frac{1}{R_2\left(\frac{1}{R_2 Y_0}\right)^{1/n}} = \frac{(R_2 Y_0)^{1/n} Y_o}{R_2 \quad Y_o}$$

$$= Y_o (R_2 Y_0)^{\frac{1-n}{n}}, \tag{16}$$

where $\omega_{\max}$ represents the frequency of the maximum value for $-Z''$ in the Nyquist plot and τ is the relaxation constant associated. The circuit element values required for fitting the impedance spectra are given in Table 4.

From data of Table 4 and values for C_{CPE} of uninhibited steel obtained showed that a reduction in capacitance values with inhibitor presence and later increasing with higher inhibitor concentration, this behaviour was related to compactness of the corrosion inhibitor protective film and the fact that coverage raise sharply with inhibitor concentration. On the other hand, DMetEtBAmBr, DMetEtBAmLau and DMetEtBAmAc higher values of C_{CPE} were linked with cation structure that allows superior coverage, a smaller thickness of inhibitor adsorbed layer and greater dielectric media response ε_r (Eq. 17):

$$C_{dl} = \frac{\varepsilon_0 \varepsilon_r}{e} S \tag{17}$$

ε_0 is the vacuum permittivity, ε_r is the relative permittivity of the material adsorbed on the metallic surface, S is the area covered by the adsorbate and e is the thickness of the coverage film. From Bode Plot of Phase Angle (Fig. 12a–g), it is only one time constant. From Bode Plot of Phase, the phase angle (ϕ) of uninhibited steel in acid media was shifted to lower values of ϕ for MetTImBr and TPyBr indicating that there was grater surface coverage and Transfer Charge Resistance [65]. On the other hand, Phase Angle shifting for DMetEtBAmLau was small because it was strongly influenced by its hydrophobic anion (Sect. 3.2). Besides $\phi_{\max}$ had similar values at different concentrations of DMetEtBAmBr, because the phase angle (ϕ) comprised the general behaviour of all patches in steel surface (Temkin adsorption isotherm, Sect. 3.2). The reduction in $\phi_{\max}$ value at a concentration of 200 ppm for MetHImBr involves spatial reorientation of adsorbed molecules onto metallic surface which produced changes in thickness adsorbed layer (e; Eq. 17; Sect. 3.2). Maximum values of $\phi_{\max}$ showed by HPyBr and MetHImBr at low concentrations was related with alkyl chain orientation causing steric hindrance. Experimental results of IE of DMetEtBAmAc fitted to Henry isotherm, therefore little change in $\phi_{\max}$ may be due high affinity between adsorbate molecules and adsorbent, till 200 ppm when transition from kinetic–diffusive process adsorption to mainly diffusive process in the adsorbed layer produced a shifting in $\phi_{\max}$ near 50° and a shifting in the frequency domain from 0.860 to 0.280 kHz.

4 Conclusions

(1) All the substituted amphiphilic compounds show good corrosion inhibition efficiency in sulphuric acid 1 M.
(2) The polarization data indicate suppression of corrosion processes in the presence of amphiphilic compounds. These inhibitors behave as cathodic type inhibitors.
(3) The inhibition is due to the adsorption of amphiphilic compounds derivatives on the steel surface and the blocking of active sites.
(4) The adsorption process is physisorption that obeys the Langmuir isotherm for MetTImBr, MetHImBr, TPyBr and HPyBr and Henry isotherm for DMetEtBAmAc. The adsorption process is chemisorption for DMetEtBAmBr that obeys Temkin isotherm.
(5) The electrochemical impedance spectroscopy spectrums showed that the mechanism of corrosion inhibition is a faradic process. Electrical equivalent circuit using a CPE describes accurately experimental findings.

Acknowledgements J.-B. Pérez-Navarrete would like to thank Consejo Nacional de Ciencia y Tecnología (CONACYT) for the scholarship awarded to carry out postgraduate studies and to N.V. Likhanova for assistance to carry out experimental work.

References

1. Wojtanowicz AK (2008) In: Orszulik ST (ed) Environmental technology in the oil industry, Springer Science-Business Media B.V., London
2. Koch GH, Brongers MPH et al (2002) FHWA-RD-01–156, Federal Highway Administration. U.S. Department of Transportation, Virginia
3. Verink ED Jr (2007) In: Cramer SD, Covino BS Jr (eds) ASM Handbook. ASM International, 13A, New York
4. Koch GH, Brongers MPH et al. (2007) In: Cramer SD, Covino BS Jr (eds) ASM Handbook. ASM International, 13A, New York
5. Galicia P, González I (2005) Electrochim Acta 50:4451
6. Revie W, Uhlig HH (2008) Corrosion and corrosion control: an introduction to corrosion science and engineering. Wiley-Interscience, New York
7. Moiseeva LS, Yupashevskii VE et al (1998) Chem Petrol Eng 34:442
8. Hackerman N, Snavely ES (1978) In: NACE basic corrosion course. NACE, Houston
9. Natishan P (2007) In: Cramer SD, Covino BS Jr (eds) ASM Handbook. ASM International, 13B, New York
10. Negm NA, Mohamed AS (2004) J Surf Deterg 7:23
11. Müller B, Oughurlian C et al (2000) Corros Sci 42:577
12. Free ML (2004) Corros Sci 46:3101
13. Stark KR, Seddon A et al (2000) Pure Appl Chem 72:2275
14. Glenn AG, Jones PB (2004) Tetrahedron Lett 45:6967
15. Kadilkar BM, Rebeiro GL (2002) Org Proc Res Dev 6:826
16. Deetlefs M, Seddon KR (2003) Green Chem 5:181
17. Fraga-Dubreuil J, Famelart MH et al (2002) Org Proc Res Dev 6:374

18. Law MC, Wong KY et al (2002) Green Chem 4:328
19. Ahluwalia KL, Parashar RK (2005) Organic reactions mechanism. Alpha Science International Ltd, Delhi
20. Welton T (1999) Chem Rev 99:2071
21. Fredlake CP, Crosthwaite JM et al (2004) Chem Eng Data 49:954
22. Fuchs-Godec R (2006) Colloid Surf A 280:130
23. Branzoi V, Branzoi F et al (2000) Mater Chem Phys 35:288
24. El-Maksoud SAA (2008) Int J Electrochem Sci 3:528
25. Migahed MA, Abd-El-Raouf AM et al (2006) J Appl Electrochem 36:395
26. Migahed MA, Nassar IF (2008) Electrochim Acta 53:2877
27. Wang L (2008) Corros Sci 48:608
28. Keles H, Keles M et al (2008) Colloid Surf A 320:138
29. Yana Y, Li W et al (2008) Electrochim Acta 53:5953
30. Abd-El-Rehim SS, Amin MA et al (2008) Mater Chem Phys 112:898
31. Khaleda KF, Al-Qahtanib MM (2009) Mater Chem Phys 113:150
32. Mansfeld F (2005) Corros Sci 47:3178
33. Konig U, Beier M et al. (1990) Proceedings of the 7th European Symposium on Corrosion Inhibitions 9, pp. 961
34. Bockris JOM, Despic A et al (1961) Electrochim Acta 4:325
35. Drazic DM (1989) In: Bockris JOM, Conway BE (eds) Modern aspects of electrochemistry. Plenum Press, New York
36. Sherif ESM, El Shamya AM et al (2007) Mater Chem Phys 102:231
37. Mansfeld F (2009) J Solid State Electrochem 13:515
38. Migahed MA (2005) Prog Org Coat 54:91
39. Jovancicevic V, Yang B et al (1998) J Electrochem Soc 135:94
40. Anand RR, Hurd RM et al (1965) J Electrochem Soc 112:138
41. Vermilyea DA (1971) Ann Rev Mater Sci 1:373
42. Oguzie EE, Unaegbu C et al (2004) Mater Chem Phys 84:363
43. Bellman C (2008) In: Stamm M (ed) Polymer surfaces and interfaces. Springer, Berlin
44. Langmuir I (1932) J Am Chem Soc 54:2798
45. Langmuir I (1918) J Am Chem Soc 40:1361
46. Langmuir I (1916) J Am Chem Soc 38:2221
47. Langmuir I (1917) J Am Chem Soc 39:1848
48. Parsons R (1959) Trans Faraday Soc 55:999
49. Tvardovski A, Tondeur D et al (2003) J Colloid Interface Sci 265:239
50. Bard AJ, Faulkner LR (2001) Electrochemical methods. Wiley, New York
51. Le Mehaute A, Crepy G (1983) Solid State Ionics 9:17
52. Zhang L, Kappl M et al (2008) Prog Colloid Polym Sci 134:39
53. Yang CH (1993) J Phys Chem 97:7097
54. López-Garzón FJ, Fernandez-Morales FJ et al (1987) Chromatography 23:97
55. Yashkin SN, Schuster RH (2003) Russ Chem Bull Int Ed 52:2360
56. Filippov LK, Silebi CA et al (1995) Langmuir 11:872
57. Pajkossy T (2005) Solid State Ionics 176:1997
58. Kerner Z, Pajkossy T (2000) Electrochim Acta 46:207
59. Pajkossy T (1997) Solid State Ionics 94:123
60. Epelboin I, Keddam M et al (1972) J Appl Electrochem 2:71
61. Chechirlian S, Keddam M (1993) In: Scully JR, Silverman DC et al (eds) Electrochemical impedance: analysis and interpretation. ASTM, Fredericksburg
62. Kiel M, Bohlen O et al (2008) Electrochim Acta 35:7367
63. Cole KS, Cole RH (1941) J Chem Phys 9:341
64. Urquidi-Macdonald M, Real S et al (1990) Electrochim Acta 35:1559
65. Kissi M, Bouklah M et al (2006) Appl Surf Sci 252:4190